AIAA'87

AIAA-87-0303

Particle-Laden Swirling Free Jets: Measurements and Predictions

D.L. Bulzan, NASA Lewis Research Center, Cleveland, OH; J.-S. Shuen, Sverdrup Technology, Inc., Lewis Research Center, Cleveland, OH; and G.M. Faeth, The University of Michigan, Ann Arbor, MI

AIAA 25th Aerospace Sciences Meeting

January 12-15, 1987/Reno, Nevada

NASA Technical Memorandum 88904
AIAA-87-0303

Particle-Laden Swirling Free Jets: Measurements and Predictions

D.L. Bulzan
Lewis Research Center
Cleveland, Ohio

J.-S. Shuen
Sverdrup Technology, Inc.
Lewis Research Center
Cleveland, Ohio

and

G.M. Faeth
The University of Michigan
Ann Arbor, Michigan

Prepared for the
25th Aerospace Sciences Meeting
sponsored by the American Institute of Aeronautics and Astronautics
Reno, Nevada, January 12-15, 1987

NASA

PARTICLE-LADEN SWIRLING FREE JETS: MEASUREMENTS AND PREDICTIONS

D.L. Bulzan
National Aeronautics and Space Administration
Lewis Research Center
Cleveland, Ohio 44135

J.-S. Shuen*
Sverdrup Technology, Inc.
Lewis Research Center
Cleveland, Ohio 44135

and

G.M. Faeth**
The University of Michigan
Ann Arbor, Michigan 48109-2140

Abstract

A theoretical and experimental investigation of single-phase and particle-laden weakly swirling jets was conducted. The jets were injected vertically downward from a 19 mm diameter tube with swirl numbers ranging from 0 to 0.33. The particle-laden jets had a single loading ratio (0.2) with particles having an SMD of 39 μm. Mean and fluctuating properties of both phases were measured using nonintrusive laser based methods while particle mass flux was measured using an isokinetic sampling probe. The continuous phase was analyzed using both a baseline k-ε turbulence model and an extended version with modifications based on the flux Richardson number to account for effects of streamline curvature. To highlight effects of interphase transport rates and particle/turbulence interactions, effects of the particles were analyzed in three ways, as follows: (1) locally homogeneous flow (LHF) analysis, where interphase transport rates are assumed to be infinitely fast; (2) deterministic separated flow (DSF) analysis, where finite interphase transport rates are considered but particle/turbulence interactions are ignored; and (3) stochastic separated flow (SSF) analysis, where both effects are considered using random walk computations.

Nomenclature

a	acceleration of gravity
C_D	drag coefficient
C_i	parameters in turbulence model
d	injector diameter
d_p	particle diameter
f	particle mass fraction
G	particle mass flux
k	turbulence kinetic energy
L_e	dissipation length scale
m_p	particle mass
n	number of particle groups
n_i	number of particles per unit time in group i
p	pressure
r	radial distance
R	injection tube radius
Re	Reynolds number
S_ϕ	source term
$S_{p\phi}$	source term due to particles
t	time
t_e	eddy lifetime
u	axial velocity
v	radial velocity
V_j	volume of computational cell j
w	angular velocity
x	axial distance
$\vec{x}_p$	particle position vector
Δx_p	relative path length of particles in an eddy
Δt_p	time of particle residence in an eddy
ϵ	rate of dissipation of turbulence kinetic energy
μ_t	turbulent viscosity
ρ	density
σ_i	turbulent Prandtl/Schmidt number
ϕ	generic property

*Senior research engineer; member AIAA.
**A.B. Mondine Professor of Aerospace Engineering; associate fellow AIAA.

Subscripts

c centerline quantity

p particle property

o injector exit condition

∞ ambient condition

m maximum value

Superscripts

( )' root-mean-square fluctuating quantity

($\bar{}$) time averaged value

($\vec{}$) vector quantity

($\tilde{}$) Favre averaged value

Introduction

Multiphase flows are extremely important in many practical devices. In a gas turbine engine, for example, fuel is sprayed into a highly turbulent, recirculating flowfield, where it evaporates and takes part in chemical reactions. Particle-laden flows are being studied as a step toward a better understanding of complex multiphase flows such as those in future advanced air-breathing engines. Particle-laden flows allow the study of interactions between the continuous and dispersed phases without interference from vaporization or combustion effects. The objective of this investigation was to extend previous work on free particle-laden jets to consider effects of swirl, which is an important aspect of many practical sprays. The performance of typical two-phase flow models of this problem was of particular interest.

Single-phase swirling jets have been studied several times in the past.[1-4] These flows are normally characterized by their swirl number. For a free jet in stagnant surroundings, the swirl number can be expressed as follows:

$$S = \frac{\int_0^\infty \tilde{\rho}\tilde{u}\tilde{w} r^2 \, dr}{R \int_0^\infty \left\{ \tilde{\rho}\tilde{u}^2 + (\bar{p} - \bar{p}_\infty) \right\} r \, dr} \qquad (1)$$

where S is an invariant of these flows.[5] For swirl numbers greater than roughly 0.6, the adverse pressure gradient set up by the decay of angular velocity causes reversal of the streamwise velocity and formation of a zone of recirculation along the axis. However, even at lower swirl numbers, the presence of swirl has large effects on the structure of a jet. For example, increasing swirl numbers cause increased rates of jet growth, entrainment of ambient fluid, and decay of streamwise velocity.

Earlier theoretical and experimental investigations of particle-laden jets have recently been reviewed;[6] therefore the present discussion of past work will be brief. The present study is an extension of earlier investigations[7-10] involving analysis and experiments for particle-laden jets. Three methods of analyzing multiphase flows were considered, as follows: (1) a locally homogeneous flow (LHF) model, where properties of both phases were taken to be the same; (2) a deterministic separated flow (DSF) model, where finite interphase transport was considered but effects of turbulence on particle motion were ignored; and (3) a stochastic separated flow (SSF) model where effects of both finite interphase transport rates and turbulence on particle motion were considered using random sampling techniques. In general, the LHF and DSF models over- and underestimated rates of particle spread and flow development, respectively. In contrast, the SSF model yielded encouraging predictions of flow structure except at high particle mass loadings, where effects of particles on turbulence properties (termed turbulence modulation by Al Taweel and Landau[11]) which were not considered in the theory, were felt to be responsible for the deficiency.

In the present investigation, the results of the previous studies were extended to particle-laden, weakly swirling jets. Relatively few theoretical studies treating particle-laden swirling flows have been published. Hamed[12] modeled the trajectories of solid particles in a flow downstream of swirl vanes. Dring and Suo[13] calculated particle trajectories in a free-vortex flow. Effects of turbulence on the particle trajectories, however, were not considered in either of these studies. Furthermore, no previous experimental studies of particle-laden jets with swirl could be found in the literature.

Due to the absence of existing measurements, the present experimental study was conducted to obtain data that could be used to assess the previously described models in a swirling flowfield. In order to obtain significant interaction between phases, relatively small solid particles (with an SMD of 39 μm) were used. Emphasis was placed on obtaining gas-phase velocities in the presence of particles, without signal interference from the particles. Initial conditions were measured near the jet exit. Single-phase jets were also studied to establish baseline results, prior to treating the particle-laden flows.

Experimental Methods

Test Apparatus

Both the single-phase and particle-laden jets were directed vertically downward within a large (1.8 m-square x 2.4 m high) screened enclosure. The injector could be traversed vertically within the enclosure while the enclosure and injector could be traversed together in the two horizontal directions. This arrangement allowed rigid mounting of all optical instrumentation used during the study.

The jet tube had an inside diameter of 19 mm and extended vertically downward for 100 injector diameters. Swirl was generated by injecting air tangentially through four 9.5 mm long slots, located 74.6 mm upstream of the jet exit. The swirl number was changed by varying the amount of air injected through the tangential slots. The air flowing through the injector tube was filtered. Both the swirl and main air streams were metered with calibrated, critical-flow orifices. The solid glass particles used during the study

were injected into the flow far upstream of the injection tube using a vibrating, variable-speed screw feeder. Particle properties and test conditions are summarized in Table I.

Instrumentation

Gas velocity. Mean and fluctuating gas velocities in the single-phase jets were measured with a two-channel (frequency shifted on both channels) Ar-Ion laser velocimetry (LV) system. The backscatter mode was used with a collecting/receiving lens focal length of 750 mm. A beam expansion ratio of 3.75 was used to improve signal-to-noise ratio. Both the jet and the ambient surroundings inside the enclosure were seeded (with 1 μm nominal diameter aluminum oxide particles) to eliminate concentration bias near the edge of the jet. Two horizontal traverses, 90° apart, at each axial position yielded all required velocity components, since two velocity components were measured simultaneously.

Gas-phase velocities were measured in the presence of particles using a single-component phase-doppler anemometer, described in detail by Bachalo and Houser.[14] With this instrument, particle size and velocity were measured simultaneously. Gas-phase velocity was measured by seeding the particle-laden jet and ambient surroundings with 1 μm nominal aluminum oxide particles and using the velocity measured for this size range to represent the continuous phase. The green (514.5 nm) line of the Ar-Ion laser was used with a 602.4 mm focal-length lens. To reduce the size of the probe volume, a beam expansion ratio of 3 was used. The receiving optics were mounted 30° off-axis in the forward scatter direction, with scattered light collected using a 495 mm focal-length lens. Since frequency shifting was not available for this system; measurement of radial and angular velocities were not performed, and only mean and fluctuating axial velocities are reported.

Particle velocity. Particle velocities were measured using the two-component LV system used for the single-phase flows, except that the receiving optics were placed off-axis approximately 30° in the forward scatter direction. The collecting lens for the receiving optics had a focal length of 602.4 mm and frequency shifting was used for both channels. Present data are number averages over all particle sizes. During the particle velocity measurements, seeding particles were not introduced into the flow and both laser power and detector gain were reduced to further insure that only signals from the test particles were observed. At each axial position, two traverses, 90° apart, yielded all required velocity components.

Particle mass flux. Particle mass flux was measured using an isokinetic sampling probe. Samples were collected on filter paper for a timed interval and weighed. Probes having inside diameters of 2 and 5 mm were used to insure adequate resolution and reasonable sampling times in various regimes of the flow. Measured particle mass fluxes integrated across the jet were within ±10 percent of the calibrated particle flow rate at all axial locations.

Theoretical Methods

General Description

The analysis is limited to steady, axisymmetric, dilute, solid-particle-laden, weakly swirling turbulent jets in an infinite stagnant media. The swirl number, calculated from Eq. (1) is restricted to values less than approximately 0.5 to prevent any zones of recirculation. The boundary-layer approximations are adopted, however, the radial pressure gradient, which is usually neglected in the boundary-layer analysis, is considered. A k-ε turbulence model is used to provide closure since it has modest computational requirements. Effects of streamline curvature on the k-ε model are considered. The injector exit Mach number is less than 0.3; therefore the kinetic energy and viscous dissipation of the mean flow are neglected with little error.

Three methods of treating multiphase flow, typical of current practice, are considered. The methods are: (1) locally homogeneous flow (LHF), where interphase transport rates are assumed to be infinitely fast and the flow can be treated like a single-phase, variable-density fluid; (2) deterministic separated flow (DSF), where finite interphase transport rates are considered but the dispersed phase is assumed to interact only with mean properties of the continuous phase; and (3) stochastic separated flow (SSF), where interphase transport rates and effects of turbulent dispersion of the dispersed phase are treated. All three methods will be only briefly discussed since they have been fully described elsewhere.[6-10]

Continuous Phase

Mean quantities for the continuous phase are found by solution of governing equations for conservation of mass and momentum in conjunction with second-order turbulence model equations for turbulent kinetic energy and its rate of dissipation. The volume fraction of the particle phase was neglected, since void fractions for the present flows exceeded 99.8 percent. The governing equations for the continuous phase can be put into the following general form:

$$\frac{\partial}{\partial x}\left(\bar{\rho}\tilde{u}\phi\right) + \frac{1}{r}\frac{\partial}{\partial r}\left(r\bar{\rho}\tilde{v}\phi\right) = \frac{1}{r}\frac{\partial}{\partial r}\left[r\left(\mu + \frac{\mu_t}{\sigma_\phi}\right)\frac{\partial \phi}{\partial r}\right] + S_\phi + S_{p\phi} \qquad (2)$$

The parameters ϕ, S_ϕ, and $S_{p\phi}$ appearing in Eq. (2), as well as empirical constants, are summarized in Table II. A modification to the ε equation, based on use of a flux Richardson number correction to account for the effect of streamline curvature,[15] was also studied. For this modification, $C_{\varepsilon 1}$ is replaced by

$$C_{\varepsilon 1}(1 + 0.9\, R_f) \qquad (3)$$

where

$$R_f = \frac{2\tilde{w}\frac{\partial}{\partial r}\left(\frac{\tilde{w}}{r}\right)}{\left\{\left(\frac{\partial \tilde{u}}{\partial r}\right)^2 + \left[r\frac{\partial}{\partial r}\left(\frac{\tilde{w}}{r}\right)\right]^2\right\}} \quad (4)$$

A consequence of the presence of angular velocity is that even though the standard boundary layer assumptions have been made, the radial momentum equation still must be considered:

$$\frac{\partial \tilde{p}}{\partial r} = \frac{\tilde{\rho}\tilde{w}^2}{r} \quad (5)$$

and cross-stream pressure gradients are not negligible. Because of the decay of angular velocity, the axial pressure gradient is also included.

The turbulent viscosity was calculated as usual:

$$\mu_t = C_\mu \tilde{\rho} k^2/\varepsilon \quad (6)$$

The flow leaving the injector was similar to fully developed flow and had no potential core. The boundary conditions for Eq. (2) are:

$$\phi = r\tilde{w} : r = 0, \frac{\partial \phi}{\partial r} = 0; \; r \to \infty, \phi = 0$$
$$\phi = r\tilde{w} : r = 0, r\tilde{w} = 0 ; \; r \to \infty, r\tilde{w} = 0 \quad (7)$$

Initial conditions were measured at $x/d = 0.5$. For the single-phase cases, all three mean and fluctuating velocities were measured. ε_0 was calculated from the definition of a turbulent length scale, as follows:

$$\varepsilon_0 = \frac{C_\mu k^{3/2}}{L} \quad (8)$$

where L was chosen as a fraction of the initial jet width to provide good agreement with the initial axial profile for k. Since only $\bar{u}$ and u' could be measured for the particle-laden cases, initial values of the continuous phase angular velocity were estimated by subtracting the measured particle angular momentum from the single-phase values. Single-phase initial values of k and ε were used for the particle-laden jet calculations.

Dispersed Phase (SSF Formulation)

The dispersed phase was treated by solving Lagrangian equations for the trajectories of a statistically significant sample of individual particles (n groups defined by initial position, velocity, and sample) as they move away from the injector and encounter a random distribution of turbulent eddies. This approach provides a means of treating effects of turbulent fluctuations on particle drag and dispersion as well as effects of particles on turbulence properties.

Key elements of the SSF model are the methods used to specify eddy properties and the time of interaction of a particle with a particular eddy. The present approach involves modification and extension of methods reported by Gosman and Ioannides.[16] Properties are assumed to be uniform within each eddy and to randomly change from one eddy to the next. At the start of a particle-eddy interaction, the velocity of an eddy is found by making a random selection from the probability density function (PDF) of velocity assuming an isotropic Gaussian PDF having standard deviations $(2k/3)^{1/2}$ and mean values $\bar{u}$, $\bar{v}$, and $\bar{w}$. A particle is assumed to interact with an eddy for a time which is the minimum of either the eddy lifetime or the time required for a particle to cross an eddy. These times are estimated following past practice,[7-10] assuming that the characteristic size of an eddy is the dissipation length scale

$$L_e = C_\mu^{3/4} k^{3/2}/\varepsilon \quad (9)$$

and that the eddy lifetime is

$$t_e = L_e/(2k/3)^{1/2} \quad (10)$$

Therefore, particles are assumed to interact with an eddy as long as both the time and distance of interaction satisfy the following criteria

$$\Delta t_p \le t_e, \quad \Delta \vec{x}_p \le L_e \quad (11)$$

Assumptions for particle trajectory calculations are typical of analysis of dilute particle-laden flows:[6] drag is treated empirically, assuming quasisteady flow for spherical particles with no influence of nearby particles; particle collisions are neglected; since $\rho_p/\rho > 200$ for present tests, effects of virtual mass, Bassett forces and Magnus forces are neglected with little error; and static pressure gradients are negligible. Local ambient properties are fixed by instantaneous eddy properties, as described earlier, which implicitly provides for effects of turbulent fluctuations on particle dispersion and drag.

With these assumptions, the position and velocity for each particle group can be found by integrating

$$\frac{dx_{pi}}{dt} = u_{pi} \quad (12)$$

$$\frac{du_{pi}}{dt} = \left(\frac{3\rho C_D}{4\, d_p \rho_p}\right)(u_i - u_{pi})\left|\vec{u} - \vec{u}_p\right| + a_i \quad (13)$$

where $i = 1,2,3$ and the velocities shown in these equations are instantaneous velocities for a particular eddy and particle group.[5] Since the particles used in the study were relatively round, the standard drag coefficient for solid spheres was taken as follows:[6]

$$C_D = \frac{24}{Re}\left(1 + \frac{Re^{2/3}}{6}\right), \; Re < 1000;$$
$$C_D = 0.44 \quad , \; Re > 1000 \quad (14)$$

Particle Source Terms

The interaction between particles and the continuous phase yields source terms in the governing equations for conservation of axial and angular momentum. The source terms are found by computing the net change in momentum as each particle group i passes through computational cell j

$$S_{pu_j} = V_j^{-1} \sum_{i=1}^{n} \dot{n}_i m_p \left(u_{pi_{in}} - u_{pi_{out}} \right)_j \qquad (15)$$

$$S_{prw_j} = V_j^{-1} \sum_{i=1}^{n} \dot{n}_i m_p \left(\left(rw_{pi} \right)_{in} - \left(rw_{pi} \right)_{out} \right)_j \qquad (16)$$

where $\dot{n}_i$ is the number of particles per unit time in each group.

DSF and LHF Models

DSF model. Effects of turbulent fluctuations on particle drag and dispersion as well as effects of turbulence modulation are ignored for the DSF model. Particle trajectories are found by integrating Eqs. (10) and (11), but the local mean velocity of the continuous phase replaces the instantaneous eddy velocity. Each initial condition yields a single deterministic trajectory; therefore, 1000 particle groups suffice to numerically close the solution. Effects of particle drag in the mean momentum equation are found from Eqs. (15) and (16), similar to the SSF calculations.

LHF model. This approximation implies that both phases have the same instantaneous velocity at each point in the flow; therefore, the flow corresponds to a variable-density single-phase fluid whose density changes due to changes in particle concentration. Turbulent dispersion of particles is then equivalent to that of a gas and particle inertia fully influences turbulence properties; i.e., the method implicitly accounts for effects of turbulence modulation to the extent that the no-slip assumption is correct.

The treatment of the variable-density fluid is similar to past practice,[6] however $\tilde{f}$ is defined here as the mass fraction of particles in the fluid. Measured initial values of $\tilde{f}$ were used for the LHF predictions. Through the assumption of no-slip, there is no need to compute particle trajectories and all particle source terms in the governing equations for the continuous phase are zero.

Numerical Solution

The calculations for the continuous phase were performed using a modified version of GENMIX.[18] The computational grid for the cases without swirl was similar to past work:[6-10] 33 cross-stream grid nodes and streamwise step size was limited to 5 percent of the current flow width or an entrainment increase of 5 percent - whichever was smaller. For the cases with swirl, 33 cross-stream grid nodes were also used but streamwise step size was reduced to the smaller of either 2 percent of the current flow width or an entrainment increase of 2 percent. The angular and radial momentum equations required modifications to the standard solution procedure. GENMIX utilizes an expanding grid in the streamwise direction and downstream values of r are not known before the axial momentum equation is solved. In order to preserve the marching character of the solution procedure, the angular momentum equation is solved first to obtain rw and then the radial momentum equation is integrated across the flowfield using downstream values of rw and upstream values of r. Then $\partial p/\partial x$ is calculated and a correction applied to it based on conservation of axial momentum. This procedure has been previously reported by Siddhartha.[18] It was found to conserve axial momentum within 2 percent. The dispersed phase was computed using a second-order finite-difference algorithm for both separated flow models. For the SSF model, 2000 and 4000 particle groups were tracked through the flowfield for the non-swirl and swirl cases, respectively.

Results and Discussion

Single-Phase Results

The single-phase results will only be briefly discussed since the present emphasis is on particle-laden flows. Typical results are shown to give an indication of the effect of swirl on the gas-phase flowfield. Predictions are shown both ignoring and considering the curvature correction to the dissipation equation based on the flux Richardson number.

Axial variation of flow properties. Predicted and measured mean streamwise velocity along the axis, maximum angular velocities, and turbulent kinetic energy along the axis for the single-phase jets are illustrated in Figs. 1(a) to (c). Results for swirl numbers of 0, 0.19, and 0.33 are shown on the figures. The rate of decay of streamwise velocity along the axis is increased as swirl is increased. Turbulent kinetic energy also increases quite dramatically with increasing swirl. For the $S = 0.33$ case, turbulent kinetic energy rises steeply almost immediately and peaks at an x/d of only 2 before decreasing once again. The maximum angular velocity decays quite rapidly, reaching one-half its original value in less than 2 injector diameters for $S = 0.33$. Predictions are in reasonably good agreement with the measurements at low swirl. Predictions are shown for both the standard k-ε model and the flux Richardson correction. As shown in Fig. 1(b), the curvature correction greatly increases k immediately downstream of the injector exit. However, for $S = 0.33$, the rapid rise of k near the injector exit is not predicted very well, even with the curvature correction. As shown in Figs. 1(a) and (c), the increase in k using the curvature correction increases the rate of decay of both axial and angular velocities.

Radial profiles. Radial profiles of mean and turbulence quantities at $x/d = 15$ for the jet without swirl are illustrated in Fig. 2. The jet width is predicted reasonably well, however, centerline values of k and peak values of Reynolds stress are somewhat overestimated. Radial profiles at $x/d = 30$ are not shown, however,

agreement between predictions and measurements was quite good.

Radial profiles at $x/d = 5$ for the two single-phase jets with swirl are shown in Figs. 3(a) and (b). As expected, increasing the swirl number increases the rate of spread of the jet. Turbulent kinetic energy and Reynolds stress also increase with increasing swirl at this axial location. Predictions are reasonably good with the flux corrected version yielding best agreement with measurements. Radial profiles at $x/d = 10$ for the same swirling flows are illustrated in Figs. 4(a) and (b). Findings are quite similar to those obtained at $x/d = 5$ (illustrated in Figs. 3(a) and (b)).

Particle-Laden Jets

Predictions and measurements of the particle-laden jets are discussed in the following. As discussed earlier, only mean and fluctuating axial velocities could be measured for the gas phase; therefore, it was necessary to estimate initial values of angular velocity and turbulent kinetic energy for the gas phase. Initial angular velocity of the continuous phase was estimated by subtracting the measured initial particle-phase angular momentum from the values obtained for the single-phase cases. For both swirl flows, particle-phase angular momentum was approximately 10 percent of the values measured for the single-phase cases. For the predictions shown here, initial values of k were assumed to be the same as the single-phase flows. Measured values of u' for the gas phase were approximately 20 percent lower across the entire jet width for the particle-laden cases (at the initial condition of $x/d = 0.5$) than for the corresponding single-phase flows. Predictions showed that reductions of k of 20 percent caused negligible changes in flow properties except very close to the injector. Initial values of ε for the particle-laden jet predictions were also unchanged from the single-phase cases. Only the standard k-ε model was utilized for the predictions reported in the following.

Axial variation of flow properties. Predicted and measured mean gas-phase axial velocities are shown in Fig. 5 for swirl numbers of 0, 0.16, and 0.3. For no swirl, axial velocity decays more slowly for the particle-laden flows than for the single-phase flow due to the momentum exchange from the particles. For the swirl flows, inlet swirl numbers were reduced approximately 10 percent for the particle-laden cases; therefore, a direct comparison with the single-phase measurements cannot be made. Predictions from both the SSF and LHF models are nearly identical and show good agreement with the data for both swirl flows.

Predictions and measurements of mean particle axial and maximum angular velocities as a function of streamwise distance are illustrated in Figs. 6 and 7. As expected, the LHF model overestimates the rate of decay of velocity for all cases since the particles possess significant inertia. Differences between the DSF and SSF models were small with both models giving reasonable agreement with the measurements. For both cases with swirl, particle velocity was lower than the gas phase at $x/d = 0.5$. Particle axial velocity increases due to momentum exchange from the continuous phase before finally beginning to decay, c.f. Fig. 6. It is encouraging that both separated-flow models correctly predict this behavior.

Radial variation of flow properties. The radial variation of both gasand particle-phase flow properties at $x/d = 5$ and 30 are illustrated in Figs. 8 and 9. Similar to past results,[6] gas-phase predictions are nearly identical for both the SSF and LHF models since particle loading ratio is relatively low. Predicted particle velocity shows the largest variation between models at $x/d = 5$. Here, the LHF model underestimates particle velocity while both separated-flow models are in reasonably good agreement with the data. At $x/d = 30$, shown in Fig. 9, the different physical assumptions embodied in the models are quite evident in the plot of radial mass flux. The LHF model overestimates the dispersion of particles while the DSF model clearly underestimates particle dispersion. Only the SSF model correctly predicts particle mass flux at this location. The predictions of fluctuating particle properties for the SSF model, also shown in Figs. 8 and 9 are reasonably good, however, u'_p is consistently underestimated. This is probably caused by the assumption of isotropic fluctuations in the SSF model and the monodisperse assumption in the predictions, since the injected particles have a standard deviation of 15 μm. Measured values of u' were always greater than v' and w' for the single-phase jet and it is expected that this behavior should be similar for the particle-laden jet.

Radial profiles of flow properties in the swirling, particle-laden jets are illustrated in Figs. 10 to 14. Gas phase properties at $x/d = 5$ are shown in Fig. 10 for swirl numbers of 0.16 and 0.3. Predictions using the SSF and LHF models are nearly identical and show that the width of the jet is slightly overestimated. Predictions this close to the injector are somewhat dependent upon initial conditions. Turbulence modulation by the particles, not included in these predictions, could also be a factor in the decreased width of the jet.

Radial profiles of particle properties at $x/d = 5$ are illustrated in Figs. 11(a) and (b). Both separated-flow models slightly overestimate axial and angular particle velocities because the gas phase width is overestimated. The LHF model underestimates particle velocities here since the particles have inertia and do not immediately respond to the continuous phase. Particle flux, also shown in Fig. 11, is quite different for the swirl cases than for the round jet without swirl. The swirl component has shifted the maximum flux outward from the center of the jet. Differences between the models are clearly evident in particle flux predictions. Even though initial values of particle concentration were used as initial conditions for the LHF model, the high rate of turbulent dispersion due to the no-slip assumption has caused the predicted maximum particle flux to shift to the center of the jet. This is clearly not correct. Both the SSF and DSF models predict an off-center maximum, however the predicted peak is shifted radially outward from the measured value due to the overprediction of angular velocity. The effect of turbulent dispersion is clearly important for this flow since the particles have spread much farther than the DSF model

predicts. Fluctuating particle velocities at $x/d = 5$ are also illustrated in Figs. 11(a) and (b) and show distinct differences for the two swirl numbers. For the lower swirl number, $S = 0.16$, SSF predictions for all three fluctuating velocities compare quite well with data. For the $S = 0.3$ case, however, u'_p is somewhat overestimated. For the single-phase case at $x/d = 5$, the measured peak value of u' is approximately 40 percent higher than measured for the particle-laden jet. Some of the reduction in u' is due to the reduction in swirl number caused by the introduction of particles (approx. 10 percent), however part of the reduction is thought to be due to turbulence modulation by the particles. This appears to be more important for the swirl flows.

Radial profiles of gas-phase properties at $x/d = 20$ are illustrated in Fig. 12 for both swirl flows. Predictions are in better agreement with measurements at this position than closer to the injector, although the jet width is still slightly overestimated. Predictions at $x/d = 20$ are not as sensitive to initial conditions and the swirl component has almost completely decayed. Again, there is little difference between predictions of gas-phase properties for the LHF and SSF models.

Radial profiles of particle properties for both swirl flows are illustrated in Figs. 13(a) and (b). Predictions of axial velocity are in good agreement with measurements for all three models. Predicted values of u'_p underestimate the measurements while v'_p and w'_p are in reasonably good agreement with measurements using the SSF model. Since effects of swirl have decayed at this axial location, ignoring the anisotropy of the continuous phase and using a single particle size for the predictions are the main reasons for this behavior--as discussed earlier. The particle mass flux predictions again highlight the different physical assumptions of the three models. Particle mass flux measurements indicated that between $x/d = 5$ and $x/d = 10$, the maximum mass flux shifted to the center of the jet for both swirl cases. Since angular and radial velocities have decayed to relatively small values at this distance and would tend to move particles outward, the only mechanism for transport inward is turbulent dispersion. As shown in Fig. 13(a), for the lower swirl number, the SSF model predicts this shift in mass flux. In contrast, the DSF model predicts a very narrow distribution with almost no particles at the center of the jet. For $S = 0.3$, the predicted maximum particle flux for the SSF model has not completely shifted to the center, however it is clearly evolving in this direction. Again, the DSF model predictions show the particles remaining in a narrow area. In contrast to the no-swirl case, the LHF model underestimates particle dispersion for both swirl flows at $x/d = 20$. This behavior is caused by neglecting the angular inertia of the particles which tends to transport them radially.

Conclusions

Major conclusions concerning the models that were evaluated during this investigation are as follows:

1. For single-phase weakly swirling jets, a correction to the dissipation equation, based on the flux Richardson number and designed to account for the effect of streamline curvature, gave better agreement with measurements than the standard k-ϵ turbulence model. This modification always increased predicted levels of k across the entire width of the jet which increased both the rate of spread of the jet and the rate of velocity decay with streamwise distance.

2. The SSF model, which accounts for both particle inertia and particle/turbulent interactions, yielded reasonably good results for the particle-laden jets. The prescription of eddy properties was not changed for these calculations from its original calibration.[8] The DSF model performed quite poorly for prediction of the particle mass flux distribution for the weakly swirling jets considered in this study. This suggests that turbulent dispersion of the particles was important for the present flows. For the swirling particle-laden jets, in contrast to the particle-laden jets without swirl, the LHF model underestimated the spread of the dispersed phase. Thus, the angular and radial inertia of the particles are important considerations in the mass flux distribution of the particles for the present flows.

3. For the swirling particle-laden jets, the continuous phase jet width was somewhat overestimated using the standard k-ϵ turbulence model. This is in contrast to the single-phase flows, where jet widths were underestimated with the standard k-ϵ model. Turbulence modulation, not considered in the predictions presented here, was probably a significant factor in the reduction of the jet width.

References

1. Rose, W.G., "A Swirling Round Turbulent Jet, 1-Mean-Flow Measurements," Journal of Applied Mechanics, Vol. 29, No. 4, Dec. 1962, pp. 615-625.

2. Pratte, B.D. and Keffer, J.F., "The Swirling Turbulent Jet," Journal of Basic Engineering, Vol. 94, No. 4, Dec. 1972, pp. 519-526.

3. Kerr, N.M. and Fraser, D., "Swirl. Part I: Effect on Axisymmetric Turbulent Jets," Institute of Fuel Journal, Vol. 38, No. 299, Dec. 1965, pp. 519-526.

4. Sislian, J.P., and Cusworth, R.A., "Laser Doppler Velocimetry Measurements of Mean Velocity and Turbulent Stress Tensor Components in a Free Isothermal Swirling Jet," UTIAS Report No. 281, University of Toronto, Mar. 1984.

5. Gupta, A.K., Lilley, D.G., and Syred, N., Swirl Flows, Abacus Press, Kent, 1984.

6. Faeth, G.M., "Recent Advances in Modeling Particle Transport Properties and Dispersion in Turbulent Flow," ASME-JSME Thermal Engineering Joint Conference Proceedings, Vol. 2, Y. Mori and W.J. Yang, eds., ASME, New York, 1983, pp. 517-534.

7. Shuen, J.S., Chen, L.D., and Faeth, G.M., "Evaluation of a Stochastic Model of Particle Dispersion in a Turbulent Round Jet," AIChE Journal, Vol. 29, No. 1, Jan. 1983, pp. 167-170.

8. Shuen, J.S., Chen, L.D., and Faeth, G.M., "Predictions of the Structure of Turbulent, Particle-Laden Round Jets," AIAA Journal, Vol. 21, No. 11, Nov. 1983, pp. 1483-1484.

9. Shuen, J.S., Solomon, A.S.P., Zhang, Q.F., and Faeth, G.M., "Structure of Particle-Laden Jets: Measurements and Predictions," AIAA Journal, Vol. 23, No. 3, Mar. 1985, pp. 396-404.

10. Zhang, Q.F., Shuen, J.S., Solomon, A.S.P., and Faeth, G.M., "Structure of Ducted Particle-Laden Turbulent Jets," AIAA Journal, Vol. 23, No. 7, July 1985, pp. 1123-1125.

11. Al Taweel, A.M. and Landau, J., "Turbulence Modulation in Two-Phase Jets," International Journal of Multiphase Flow, Vol. 3, No. 4, June 1977, pp. 341-351.

12. Hamed, A., "Particle Dynamics of Inlet Flow Fields with Swirling Vanes," AIAA Paper 81-0001, Jan. 1981.

13. Dring, R.P., and Suo, M., "Particle Trajectories in Swirling Flows," Journal of Energy, Vol. 2, No. 4, July-Aug. 1978, pp. 232-237.

14. Bachalo, W.D. and Houser, M.J., "Development of the Phase/Doppler Spray Analyzer for Liquid Drop Size and Velocity Characterizations," AIAA Paper 84-1199, June 1984.

15. Leschziner, M.A. and Rodi, W., "Computation of Strongly Swirling Axisymmetric Free Jets," AIAA Journal, Vol. 22, No. 12, Dec. 1984, pp. 1742-1747.

16. Gosman, A.D. and Ioannides, E., "Aspects of Computer Simulation of Liquid-Fueled Combustors," Journal of Energy, Vol. 7, No. 6, Nov.-Dec. 1983, pp. 482-490.

17. Spalding, D.B., GENMIX: A General Computer Program for Two-Dimensional Parabolic Phenomena, Pergamon Press, Oxford, 1978.

18. Siddhartha, V., "Boundary Layers with Swirl," PhD Thesis, Imperial College of Science and Technology, London, 1971.

TABLE I. - SUMMARY OF TEST CONDITIONS[a]

Parameter	Single-phase jets			Particle-laden jets		
	Case 1	Case 2	Case 3	Case 1	Case 2	Case 3
Centerline air axial velocity, m/s[b]	14.86	12.94	13.34	13.75	11.9	12.2
Maximum air angular velocity, m/s[b]	0	3.16	5.92	0	-----	-----
Swirl number[c]	0	.19	.33	0	.16	.3
Centerline particle axial velocity, m/s[b]	-----	-----	-----	13.8	10.39	10.26
Maximum particle angular velocity, m/s[b]	-----	-----	-----	0	1.48	2.26
SMD, μm[d]	-----	-----	-----	39	39	39
Loading ratio[e]	-----	-----	-----	.2	.2	.2

[a]Ambient temperature and pressures, 296.K, 97 kPa; injector inside diameter, 19 mm; particle density, 2500 kg/m^3.
[b]Measured at x/d = 0.5.
[c]Calculated from Eq. (1).
[d]The size distribution has a standard deviation of 15 μm.
[e]Ratio of injected particle mass flow rate to air mass flow rate.

TABLE II. - SOURCE TERMS IN GOVERNING EQUATIONS

ϕ	S_ϕ	$S_{p\phi}$
1	0	0
$\tilde{u}$	$-\frac{\partial \bar{p}}{\partial x}$	S_{pu}
$r\tilde{w}$	$-\frac{1}{r}\frac{\partial}{\partial r}\left\{\left(\mu + \mu_t\right) 2r\tilde{w}\right\}$	S_{pw}
$\tilde{f}$	0	0
k	$\mu_t\left\{\left(\frac{\partial \tilde{u}}{\partial r}\right)^2 + \left[r\frac{\partial}{\partial r}\left(\frac{\tilde{w}}{r}\right)\right]^2\right\} - \bar{\rho}\varepsilon$	0
ε	$C_{\varepsilon 1}\mu_t\frac{\varepsilon}{k}\left\{\left(\frac{\partial \tilde{u}}{\partial r}\right)^2 + \left[r\frac{\partial}{\partial r}\left(\frac{\tilde{w}}{r}\right)\right]^2\right\} - C_{\varepsilon 2}\bar{\rho}\frac{\varepsilon^2}{k}$	0

C_μ	$C_{\varepsilon 1}$	$C_{\varepsilon 2}$	σ_k	σ_ε	σ_f
0.09	1.44	1.87	1.0	1.3	0.7

TABLE I. - SUMMARY OF TEST CONDITIONS[a]

Parameter	Single-phase jets			Particle-laden jets		
	Case 1	Case 2	Case 3	Case 1	Case 2	Case 3
Centerline air axial velocity, m/s[b]	14.86	12.94	13.34	13.75	11.9	12.2
Maximum air angular velocity, m/s[b]	0	3.16	5.92	0	-----	-----
Swirl number[c]	0	.19	.33	0	.16	.3
Centerline particle axial velocity, m/s[b]	-----	-----	-----	13.8	10.39	10.26
Maximum particle angular velocity, m/s[b]	-----	-----	-----	0	1.48	2.26
SMD, μm[d]	-----	-----	-----	39	39	39
Loading ratio[e]	---	-----	-----	.2	.2	.2

[a]Ambient temperature and pressures, 296.K, 97 kPa; injector inside diameter, 19 mm; particle density, 2500 kg/m^3.
[b]Measured at $x/d = 0.5$.
[c]Calculated from Eq. (1).
[d]The size distribution has a standard deviation of 15 μm.
[e]Ratio of injected particle mass flow rate to air mass flow rate.

TABLE II. - SOURCE TERMS IN GOVERNING EQUATIONS

ϕ	S_ϕ	$S_{p\phi}$
1	0	0
$\tilde{u}$	$-\frac{\partial \bar{p}}{\partial x}$	S_{pu}
$r\tilde{w}$	$-\frac{1}{r}\frac{\partial}{\partial r}\left\{\left(\mu + \mu_t\right) 2r\tilde{w}\right\}$	S_{pw}
$\tilde{f}$	0	0
k	$\mu_t\left\{\left(\frac{\partial \tilde{u}}{\partial r}\right)^2 + \left[r\frac{\partial}{\partial r}\left(\frac{\tilde{w}}{r}\right)\right]^2\right\} - \bar{\rho}\varepsilon$	0
ε	$C_{\varepsilon 1}\mu_t\frac{\varepsilon}{k}\left\{\left(\frac{\partial \tilde{u}}{\partial r}\right)^2 + \left[r\frac{\partial}{\partial r}\left(\frac{\tilde{w}}{r}\right)\right]^2\right\} - C_{\varepsilon 2}\bar{\rho}\frac{\varepsilon^2}{k}$	0

C_μ	$C_{\varepsilon 1}$	$C_{\varepsilon 2}$	σ_k	σ_ε	σ_f
0.09	1.44	1.87	1.0	1.3	0.7

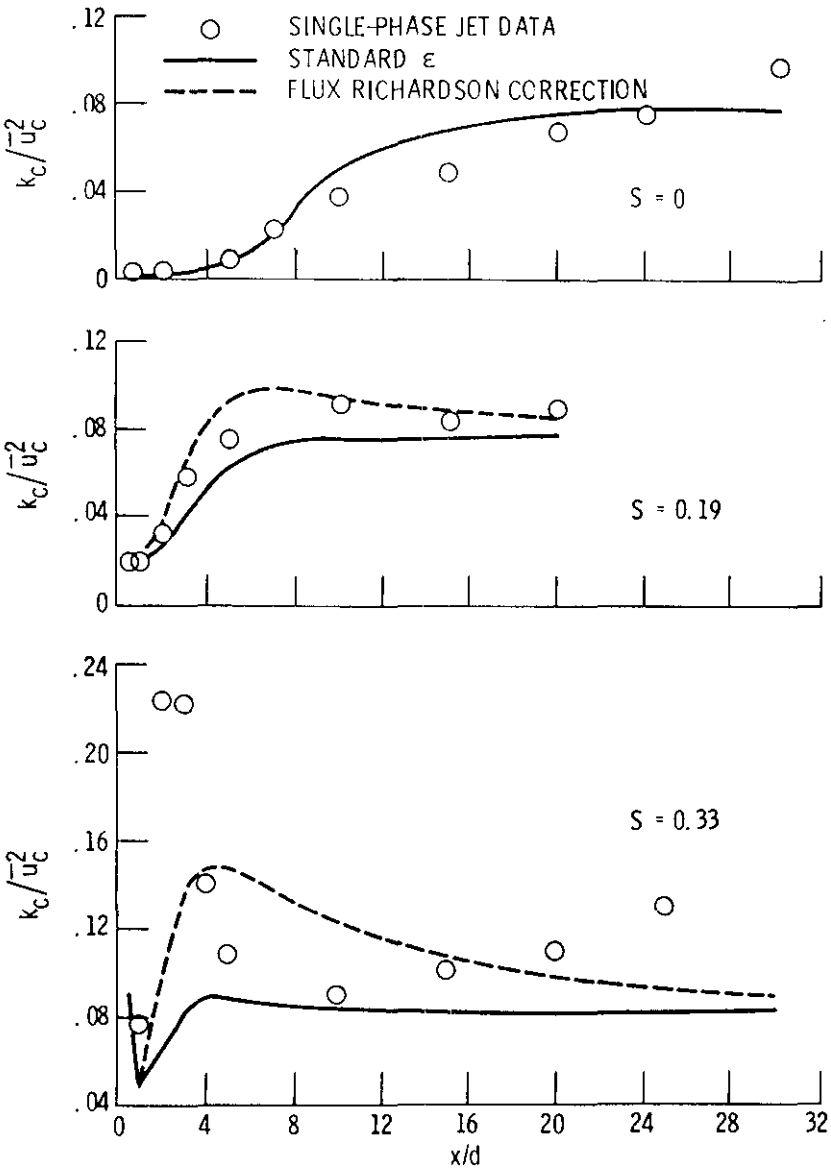

(b) Turbulent kinetic energy.

Figure 1. - Continued.

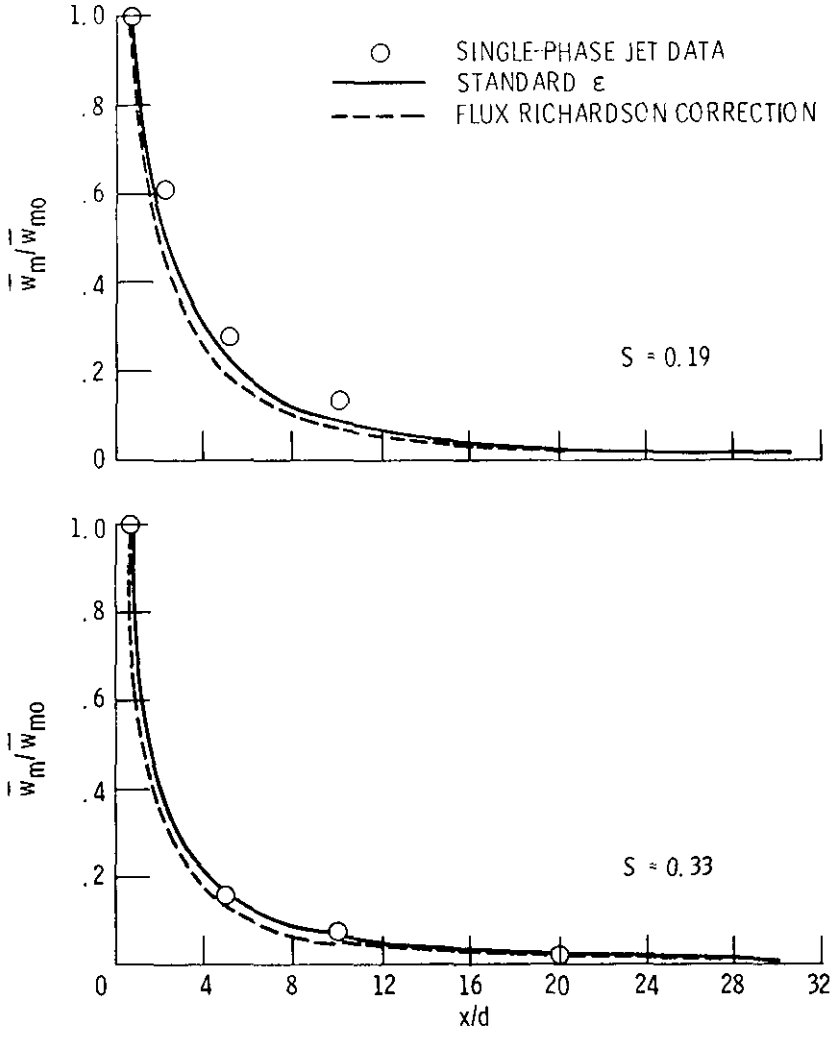

(c) Maximum angular velocities.

Figure 1. - Concluded.

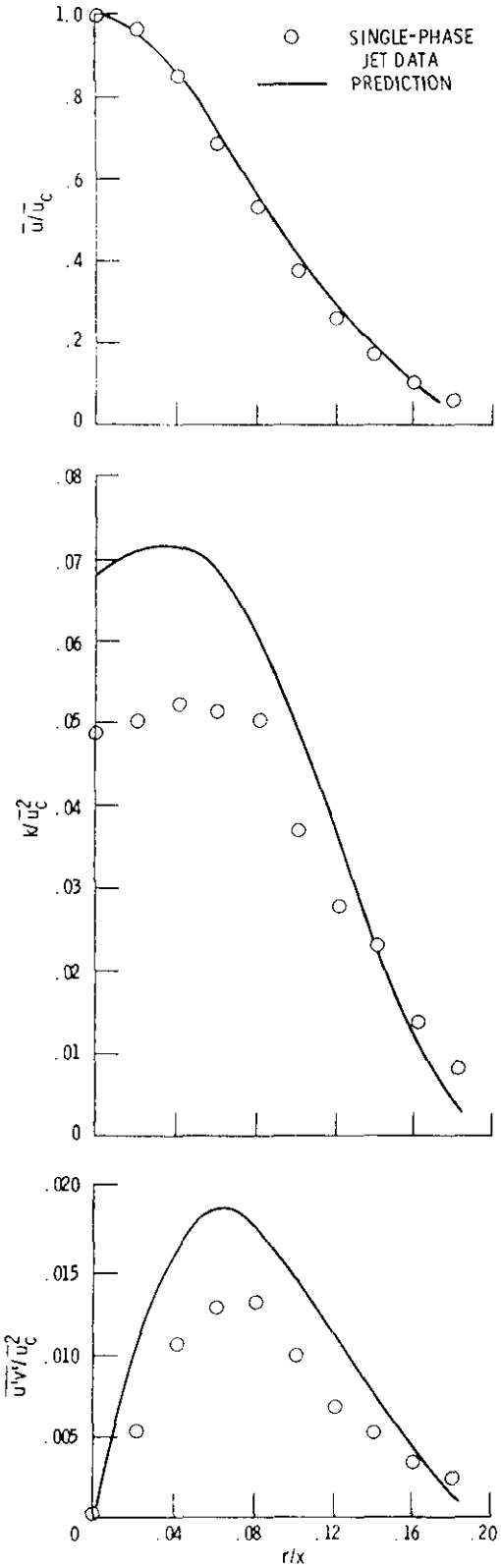

Figure 2. - Radial profiles of flow properties in the single-phase nonswirling jet at x/d = 15.

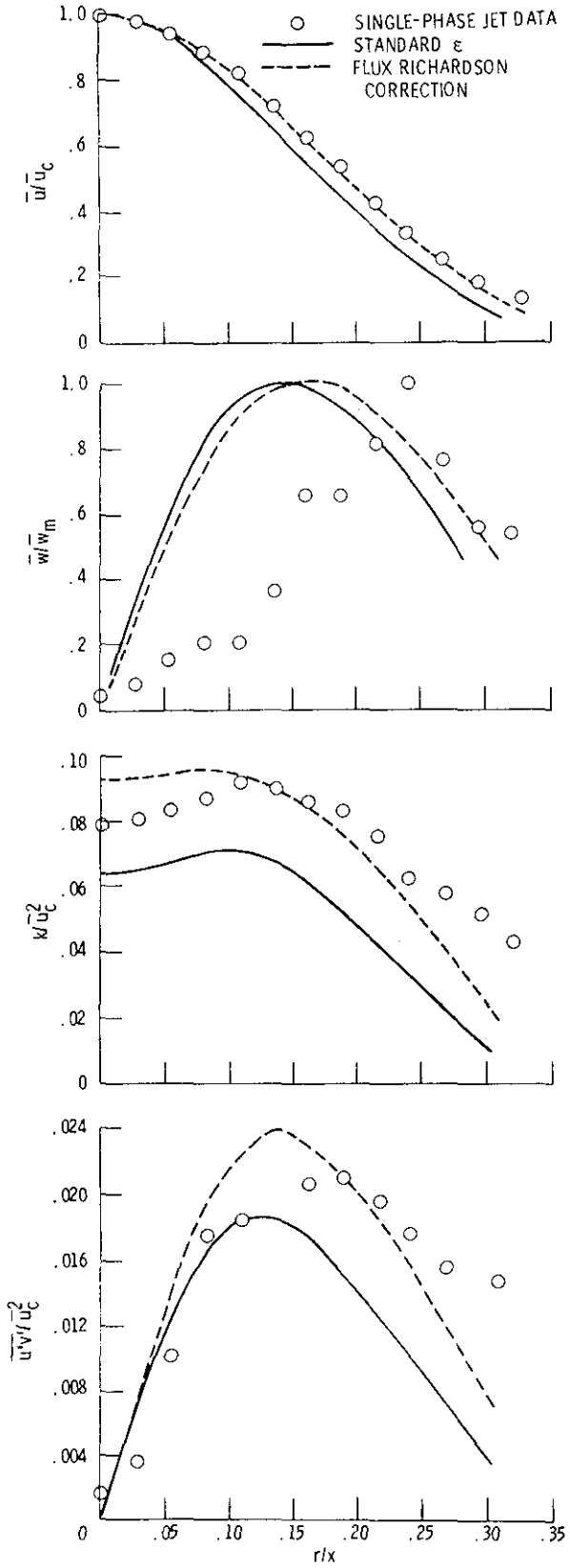

(a) S = 0.19.

Figure 3. - Radial profiles of flow properties in the single-phase swirling jets at x/d = 5.

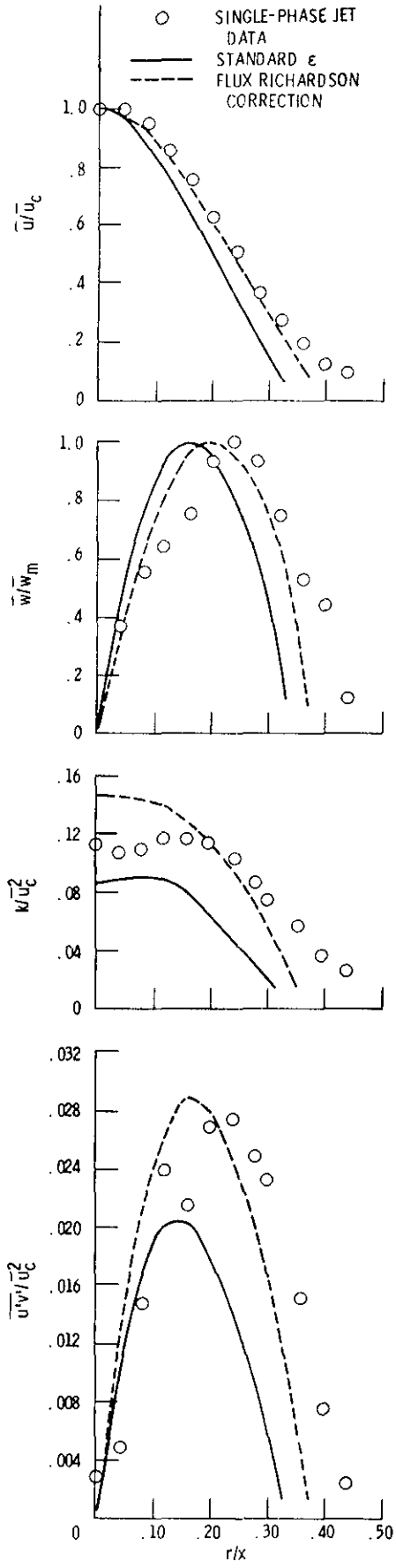

(b) S = 0.33.

Figure 3. - Concluded.

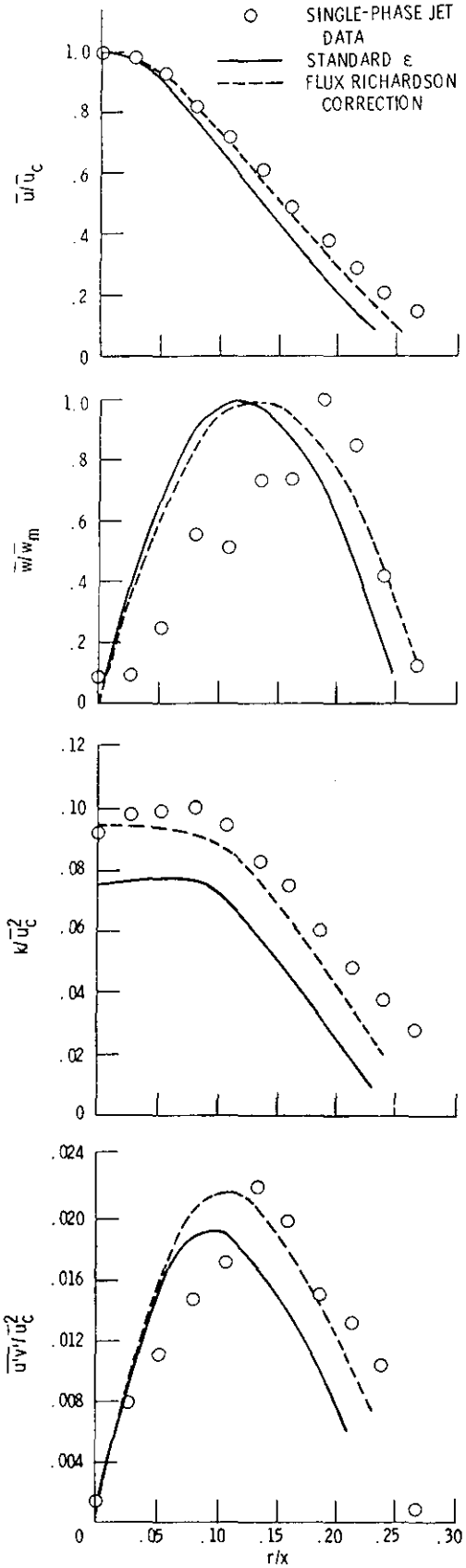

(a) S = 0.19.

Figure 4. - Radial profiles of flow properties in the single-phase swirling jets at x/d = 10.

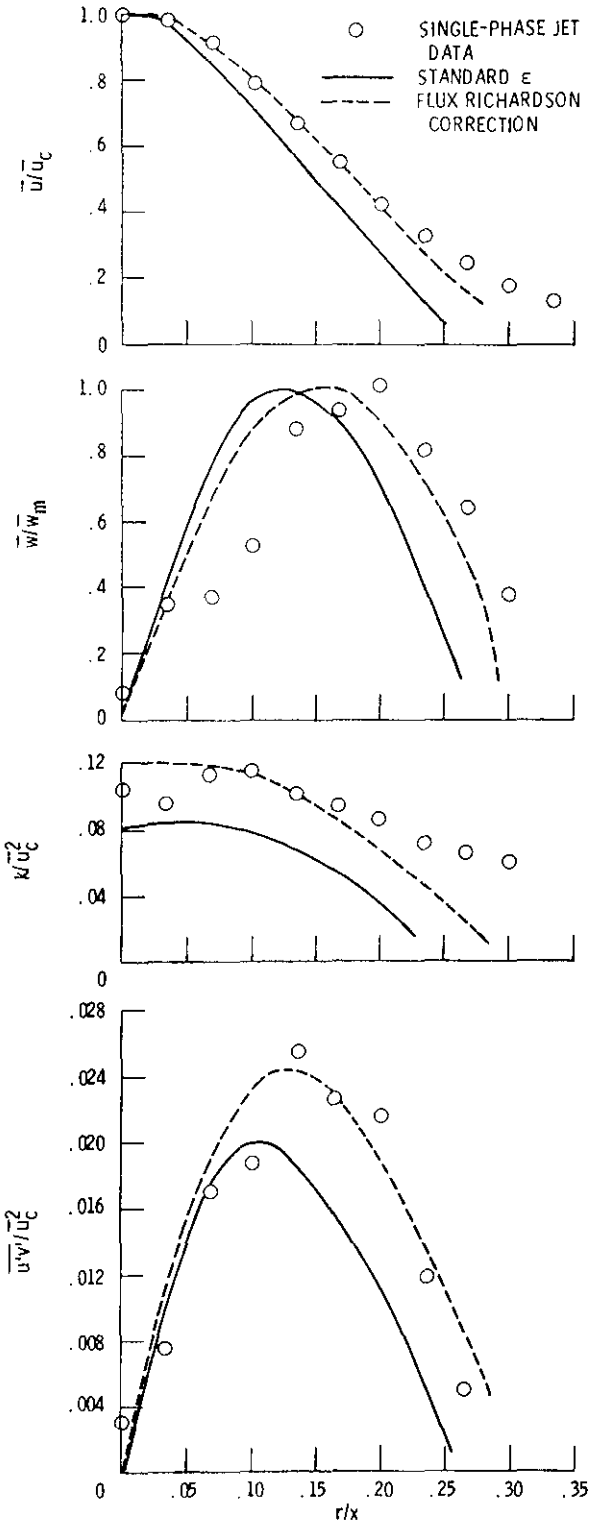

(b) S = 0.33.

Figure 4. - Concluded.

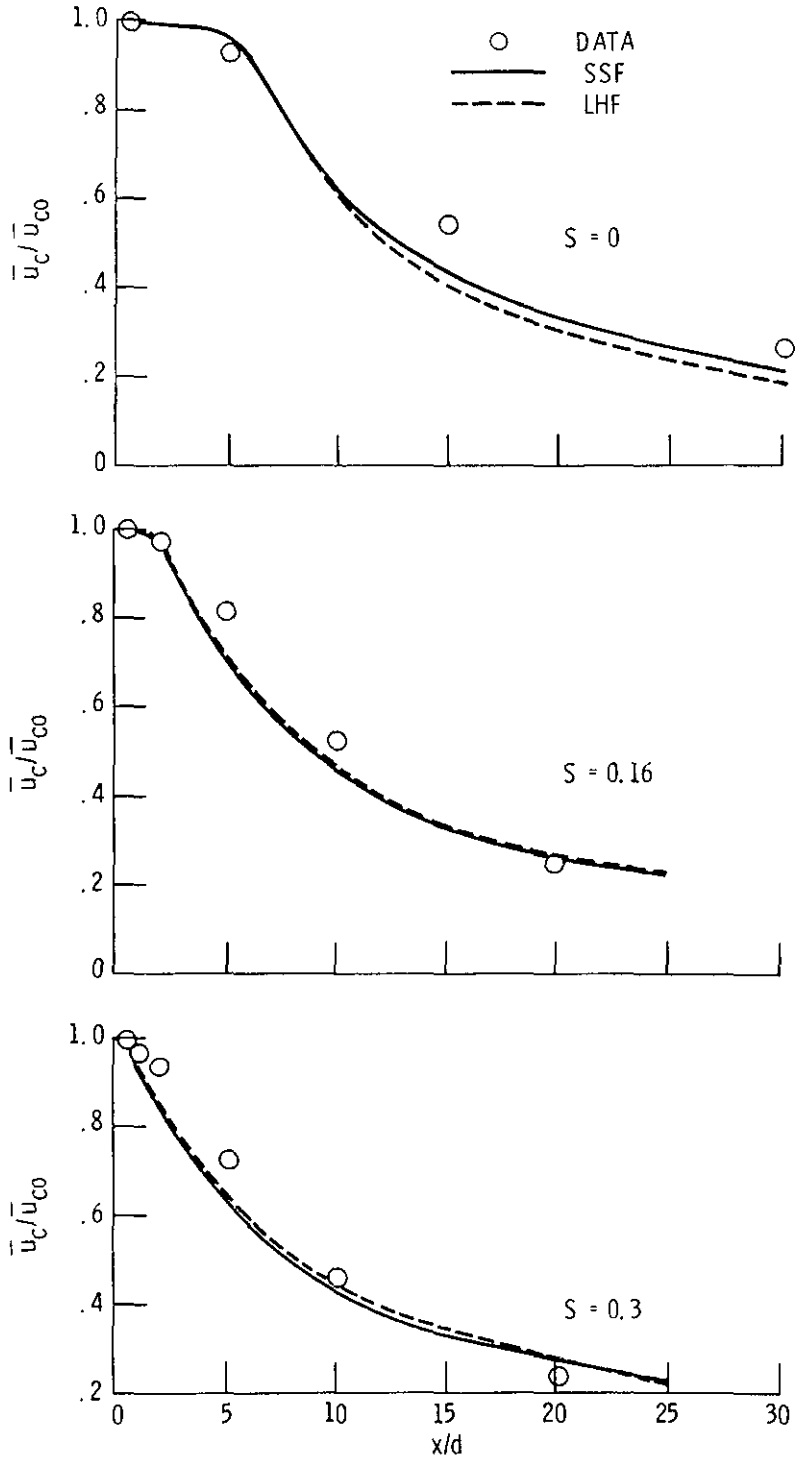

Figure 5. - Streamwise gas velocities along the axis of the particle-laden jets.

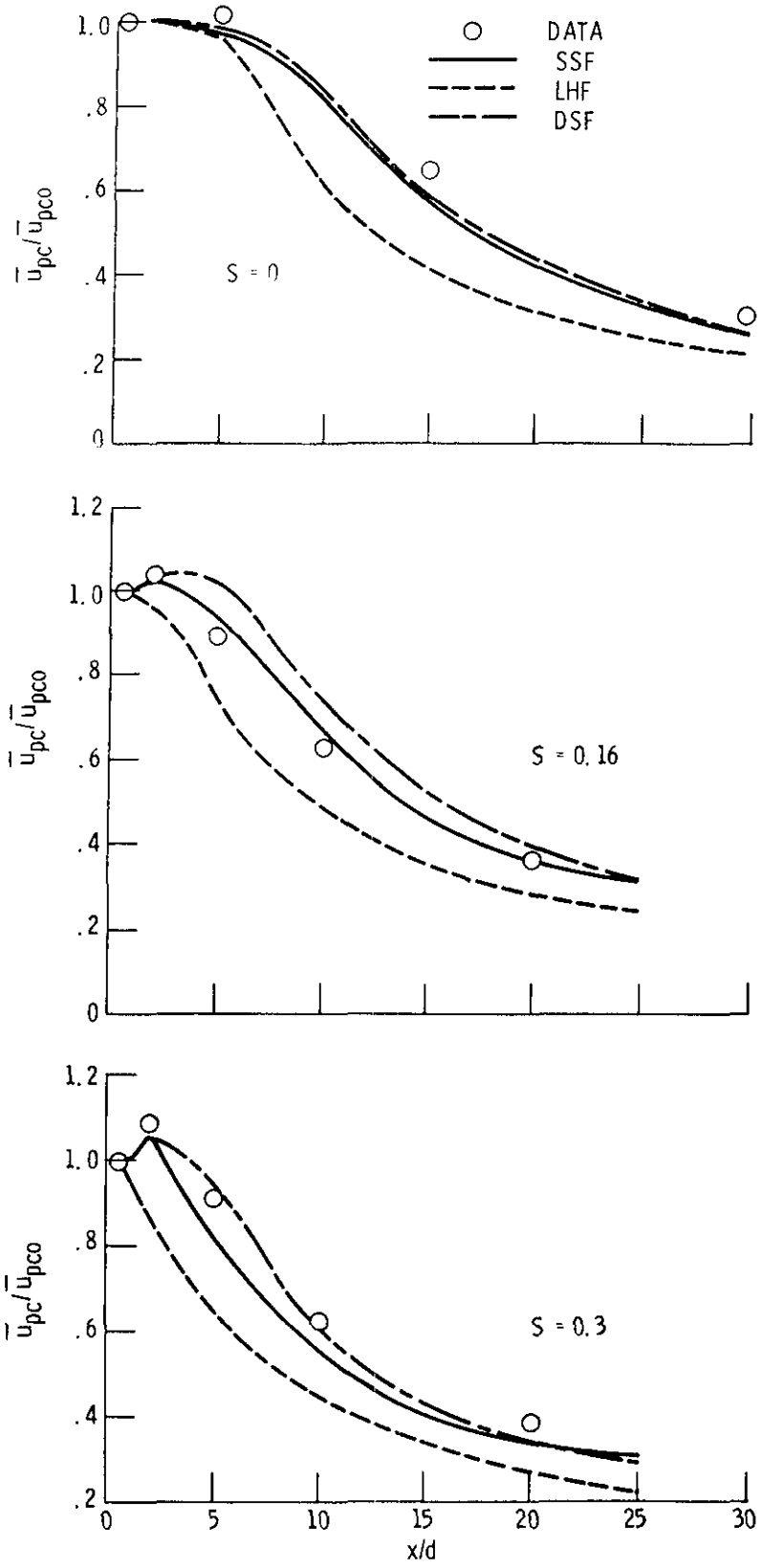

Figure 6. - Particle streamwise velocities along the axis of the particle-laden jets.

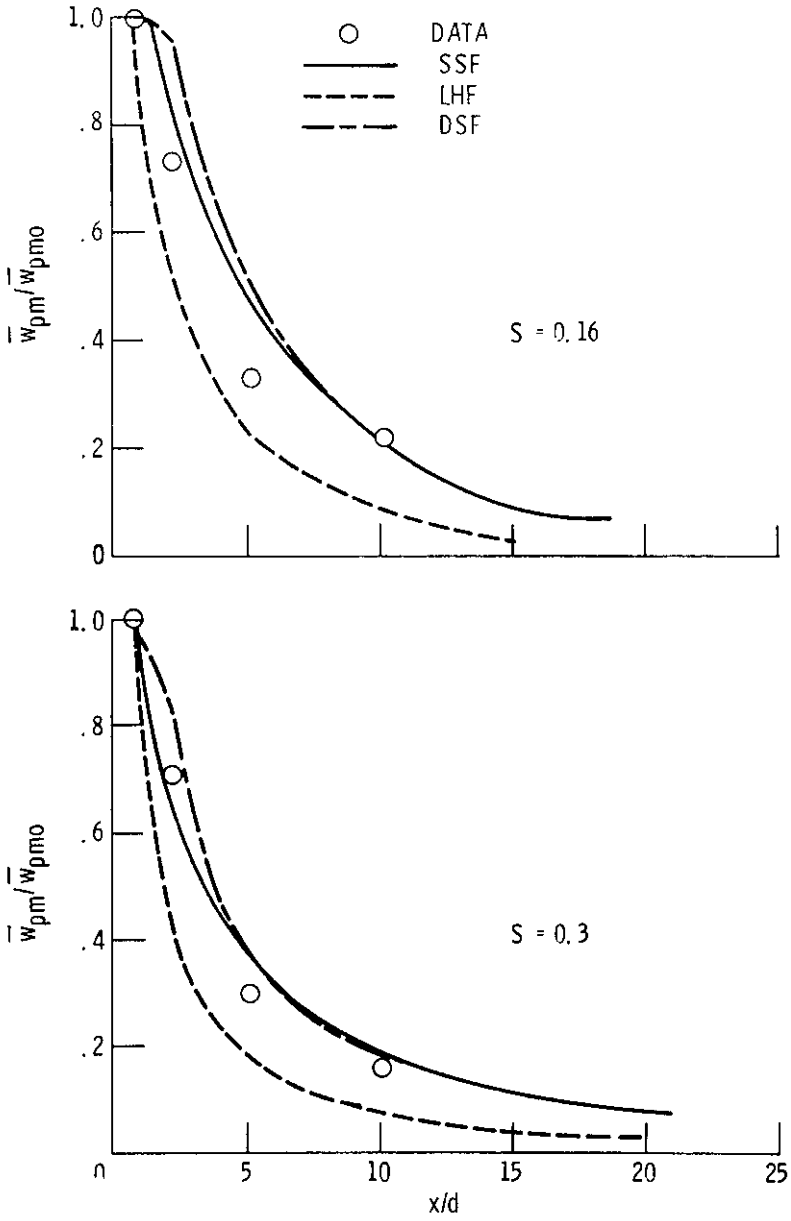

Figure 7. - Variation of maximum particle angular velocity with streamwise distance in the swirling particle-laden jets.

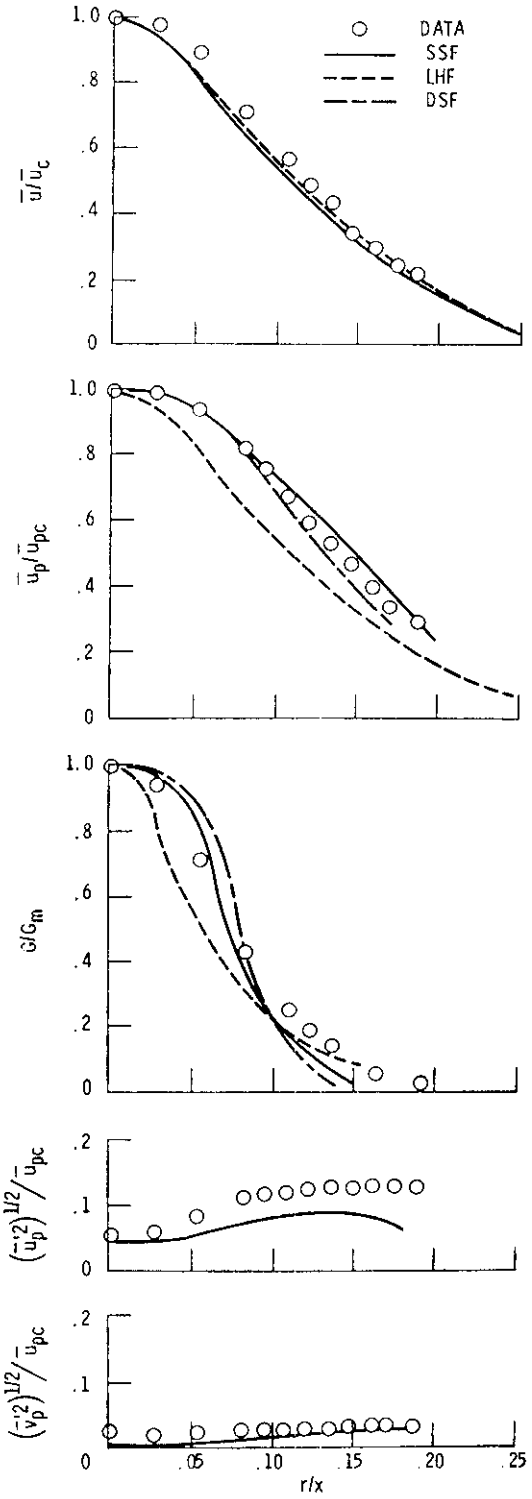

Figure 8. - Radial variation of flow properties in the nonswirling particle-laden jet at x/d = 5.

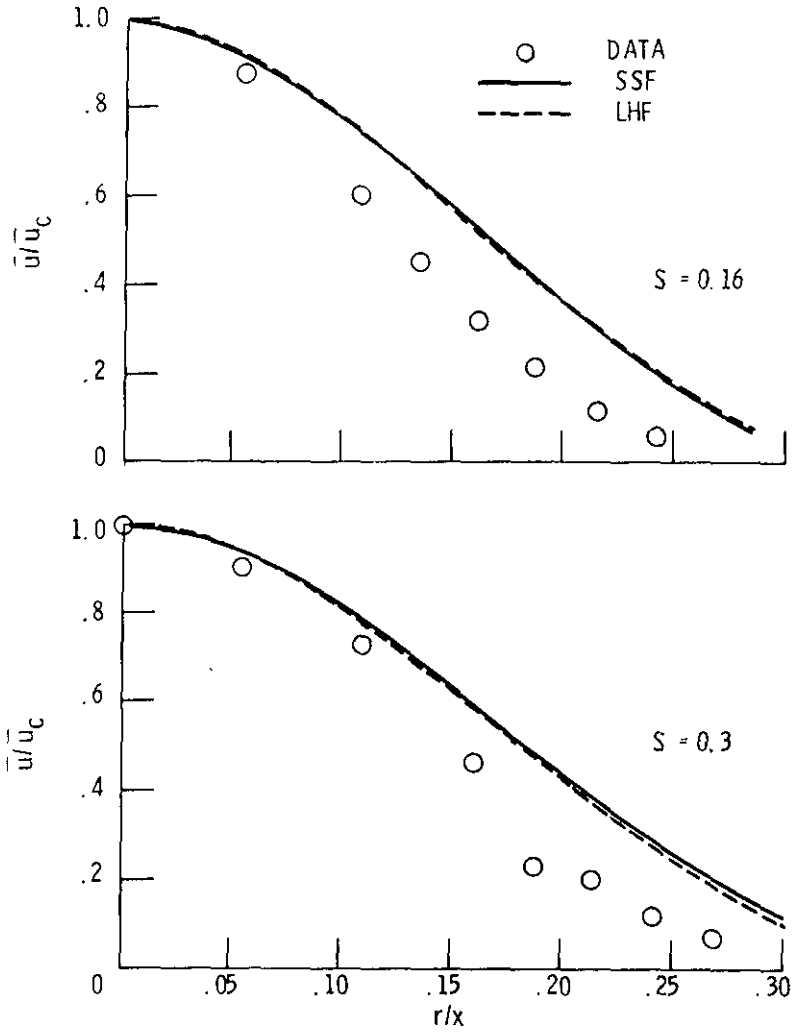

Figure 10. - Radial profiles of gas properties in swirling particle-laden jets at x/d = 5.

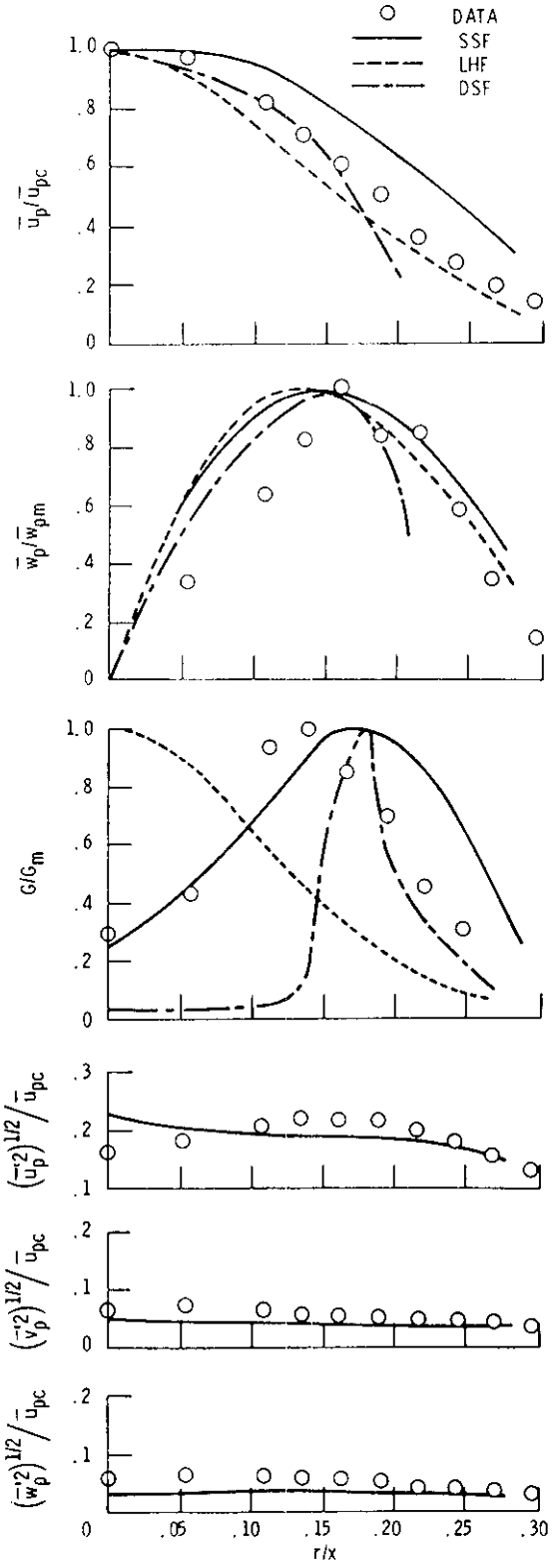

(a) S = 0.16.

Figure 11. - Radial profiles of particle properties in swirling particle-laden jets at x/d = 5.

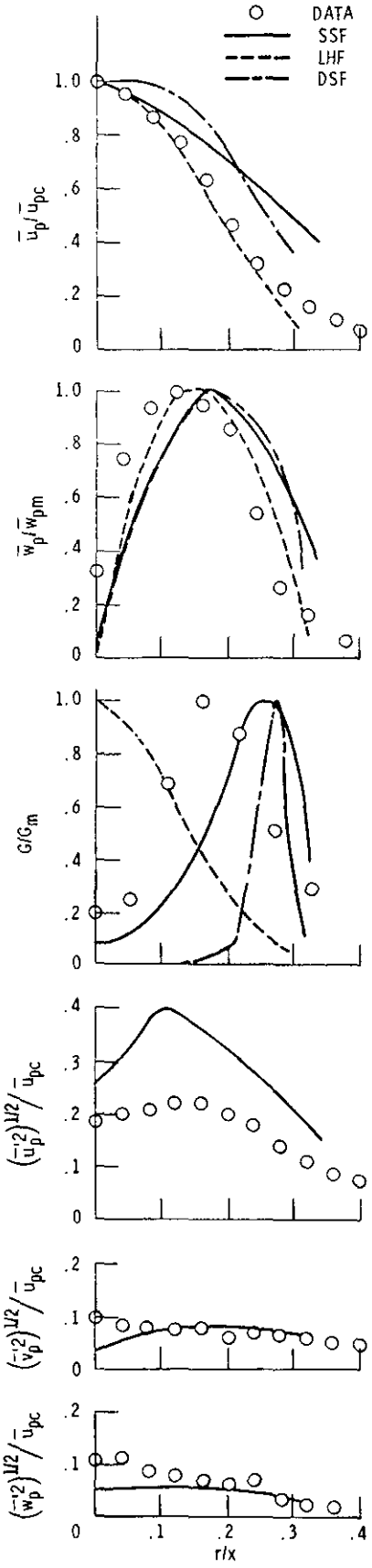

(b) S = 0.30.

Figure 11. - Concluded.

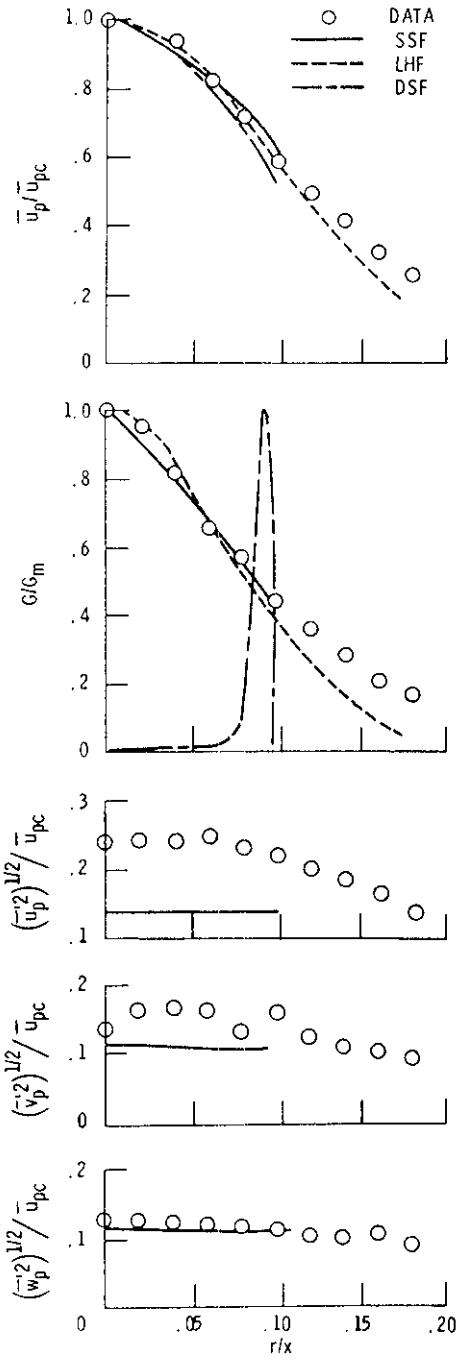

(a) S = 0.16.

Figure 13. - Radial profiles of particle properties in swirling particle-laden jets at x/d = 20.

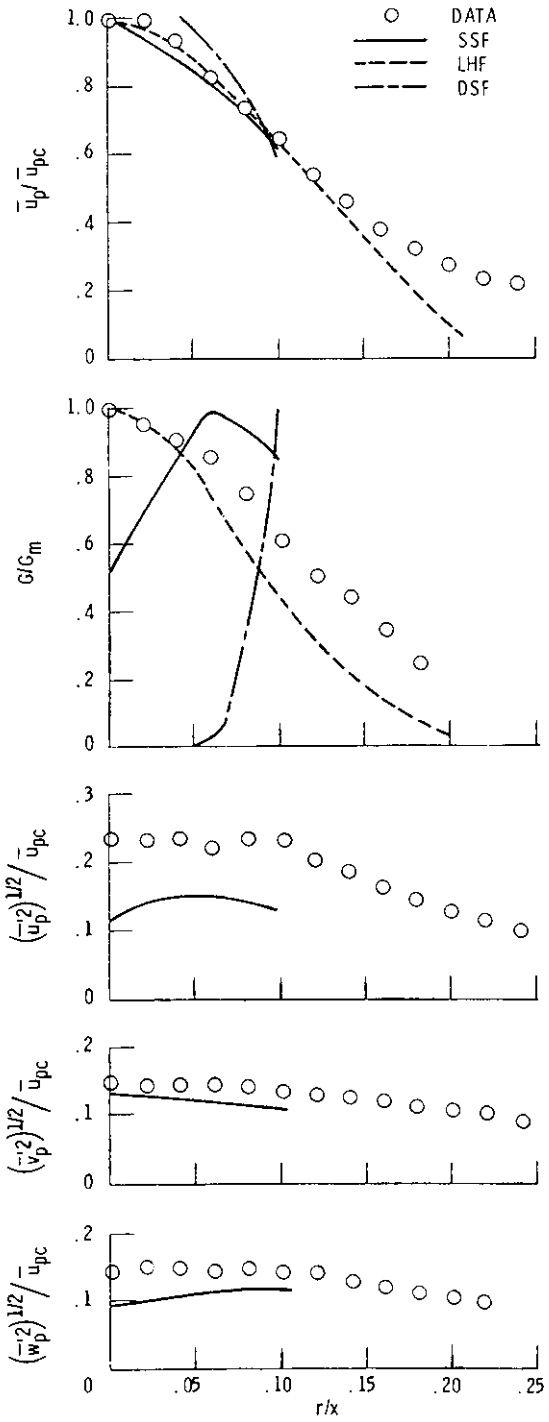

(b) S = 0.30.

Figure 13. - Concluded.

1. Report No.	2. Government Accession No.	3. Recipient's Catalog No.
NASA TM-88904 AIAA-87-0303		

4. Title and Subtitle	5. Report Date
Particle-Laden Swirling Free Jets: Measurements and Predictions	
	6. Performing Organization Code 505-62-21
7. Author(s) D.L. Bulzan, J.-S. Shuen, and G.M. Faeth	8. Performing Organization Report No. E-3307
	10. Work Unit No.
9. Performing Organization Name and Address National Aeronautics and Space Administration Lewis Research Center Cleveland, Ohio 44135	11. Contract or Grant No.
	13. Type of Report and Period Covered Technical Memorandum
12. Sponsoring Agency Name and Address National Aeronautics and Space Administration Washington, D.C. 20546	14. Sponsoring Agency Code

15. Supplementary Notes

Prepared for the 25th Aerospace Sciences Meeting, sponsored by the American Institute of Aeronautics and Astronautics, Reno, Nevada, January 12-15, 1987. D.L. Bulzan, NASA Lewis Research Center; J.-S. Shuen, Sverdrup Technology, Inc., Lewis Research Center; G.M. Faeth, The University of Michigan, Ann Arbor, Michigan 48109-2140.

16. Abstract

A theoretical and experimental investigation of single-phase and particle-laden weakly swirling jets was conducted. The jets were injected vertically downward from a 19 mm diameter tube with swirl numbers ranging from 0 to 0.33. The particle-laden jets had a single loading ratio (0.2) with particles having an SMD of 39 μm. Mean and fluctuating properties of both phases were measured using nonintrusive laser based methods while particle mass flux was measured using an isokinetic sampling probe. The continuous phase was analyzed using both a baseline k-ε turbulence model and an extended version with modifications based on the flux Richardson number to account for effects of streamline curvature. To highlight effects of interphase transport rates and particle/turbulence interactions, effects of the particles were analyzed in three ways, as follows: (1) locally homogeneous flow (LHF) analysis, where interphase transport rates are assumed to be infinitely fast; (2) deterministic separated flow (DSF) analysis, where finite interphase transport rates are considered but particle/turbulence interactions are ignored; and (3) stochastic separated flow (SSF) analysis, where both effects are considered using random-walk computations.

17. Key Words (Suggested by Author(s))	18. Distribution Statement
Swirling jets; Two-phase flows; Particle-laden jets	Unclassified - unlimited STAR Category 07

19. Security Classif. (of this report)	20. Security Classif. (of this page)	21. No. of pages	22. Price*
Unclassified	Unclassified		

*For sale by the National Technical Information Service, Springfield, Virginia 22161